Suspended sediment dynamics in a Southeast Asian mountainous catchment: Combining river monitoring and fallout radionuclide tracers

Elian Gourdin, O. Evrard, Sylvain Huon, Irene Lefevre, Olivier Ribolzi, Jean-Louis Reyss, Oloth Sengtaheuanghoung, Sophie Ayrault

*Revised Manuscript with no changes marked
Click here to view linked References

Corresponding Author: Elian Gourdin

Telephone number: +33169824362

Email address: elian.gourdin@lsce.ipsl.fr

Title:

Suspended sediment dynamics in a Southeast Asian mountainous catchment: combining river monitoring and fallout radionuclide tracers

Abstract

Soil erosion is intense in mountainous tropical regions where heavy storms result in the supply of large quantities of sediment to rivers. The origin and dynamics of suspended sediment were analysed in a catchment located in northern Laos during the first erosive flood of the rainy season in May 2012. The catchment was equipped with 4 successive gauging stations (draining areas ranging 0.2 - 11.6 km²). Fallout radionuclides (Beryllium-7 - ^{7}Be, unsupported Pb-210 -$^{210}Pb_{xs}$, and Cesium-137 -^{137}Cs) were determined on rainfall, overland flow, stream water, suspended sediment, soil surface and subsurface samples (with n = 3, 19, 75, 75, 65 and 14 respectively). Assumptions underpinning the ^{7}Be-labelling method were validated by implementing experiments in the laboratory (i.e., rainwater ^{7}Be sorption to soil particles) and in the field (i.e., ^{7}Be: $^{210}Pb_{xs}$ activity ratio evolution in rainwater and related overland flow during a natural storm event). Radionuclide analyses provided a way to quantify variations in sediment dynamics and origin throughout the flood: (1) a proportion of recently eroded sediment (labelled by ^{7}Be, and referred to as "fresh sediment") ranging between *ca.* 8 - 35% in suspended loads; (2) higher contributions of fresh sediment at the beginning of the flood rising stage; (3) a progressive dilution of fresh sediment by particles remobilised from the riverbed / channel; (4) the dominance of particles originating from the soil surface (*ca.* 70 - 80% of total sediment load) in upper parts and a much larger contribution of subsurface material (*ca.* 64%) at the downstream station. The original contribution of ^{7}Be-labelled particles derived from collapsed riverbanks to sediment export was also demonstrated. This pilot study supports the use of fallout ^{7}Be and $^{210}Pb_{xs}$ in tropical catchments to constrain sediment dynamics. It also puts forward the need to better characterize the sources of sediment in order to avoid possible misinterpretations.

1. Introduction

Soil erosion is particularly intense in mountainous subtropical regions where heavy storms may result in the supply of large quantities of suspended sediment to streams (Descroix et al., 2008; Valentin et al., 2008). Large exports of suspended matter by mountain rivers lead to numerous problems downstream (Syvitski et al., 2005). Sediments can accumulate behind dams, which results in the siltation of water reservoirs (Downing et al., 2008; Thothong et al., 2011). Suspended matter also contributes to water quality degradation (Tanik et al., 1999) and conveys biological compounds, playing thereby a major role in global nutrient biogeochemical cycles (Quinton et al., 2010). It also constitutes a potential vector for various pollutants such as metals, polycyclic aromatic hydrocarbons or faecal bacteria (Ribolzi et al., 2010; Gateuille et al., 2014).

In order to limit those negative impacts, sediment supply to rivers needs to be controlled. Design and implementation of appropriate management procedures require a better understanding of suspended matter dynamics in mountainous catchments. Their behaviour should be better constrained in time, and particularly during floods, as most riverine sediments are exported during those short periods (Meybeck et al., 2003; Mano et al., 2009). To this end, tracers that are preferentially sorbed or contained in the fine mineral and organic suspended fractions (i.e., clays and fine silts, He and Walling, 1996) may be used to follow sediment pathways across catchments (Koiter et al., 2013).

Radionuclides that are supplied to the soil surface by rainfall, i.e. beryllium-7 (^{7}Be) and unsupported or excess lead-210 (^{210}Pb$_{xs}$) are used to estimate soil erosion rates at the hillslope scale (Schuller et al., 2006; Sepulveda et al., 2008), or to characterize the temporal transfer of sediment in larger river systems (Bonniwell et al., 1999). Their different half-lives ($T_{1/2}$ = 53 days for ^{7}Be and $T_{1/2}$ = 22.3 years for ^{210}Pb$_{xs}$) are particularly relevant to differentiate between fresh sediment tagged with ^{7}Be and older remobilized sediment depleted in ^{7}Be. Based on this simple principle, Matisoff et al. (2005) proposed to calculate the ^{7}Be: ^{210}Pb$_{xs}$ activity ratio (^{7}Be/^{210}Pb$_{xs}$) in both rainwater and riverine sediment to estimate fresh sediment percentages in rivers and infer transfer times or transport distances. Alternative approaches used radionuclide mass-balance models such as the one proposed by Dominik et al. (1987) and improved by Le Cloarec et al. (2007), or associated both methods (Evrard et al., 2010). However, several limitations may arise regarding the assumptions underpinning those methods. The validity of radionuclides as tracers of sediment fluxes in large rivers has been recently questioned (Walling, 2012; Taylor et al., 2013). The main criticism focussed on the potential difference of $^{7}Be/^{210}Pb_{xs}$ activity ratio value in rainwater and in fresh sediment. This may occur when particles are tagged with radionuclides from successive storms and not with the event of investigation alone. Another concern arises from a possible misinterpretation of $^{7}Be/^{210}Pb_{xs}$ variations measured in sediment, as low values may result from various processes: radionuclide decay; desorption (when sediment remained buried in the riverbed) or changes in the source of sediment with the supply of subsurface particles (depleted in fallout radionuclides; e.g., Whiting et al., 2005). In order to reduce those uncertainties, a third fallout radionuclide, cesium-137 (^{137}Cs; $T_{1/2}$ = 30.2 years) proved to be useful to distinguish between particles originating from soil surface and exposed to atmospheric fallout of bomb tests during the second half of the 20th century (Ritchie and McHenry, 1990) and particles from the subsurface (below *ca.* 30 cm depth), protected from ^{137}Cs and ^{7}Be fallout (e.g. Olley et al., 1993; Ben Slimane et al., 2013; Evrard et al., 2013; Hancock et al., 2014).

In this study, experiments were carried out in the Houay Pano - Houay Xon nested catchments located in Laos and exposed to summer monsoon, to quantify the respective contributions of surface and subsurface soil to suspended sediment loads during an erosive flood event that took place at the beginning of the rainy season in May 2012. The fallout ^{7}Be activity of the previous rainy season should have sufficiently decayed during the 6-months dry period to become negligible compared to their recent supply at the onset of the wet season. Every compartment of the erosional system, from rainwater to stream sediment, was sampled for fallout radionuclide analyses. Adsorption experiments were also conducted for ^{7}Be at the microplot's scale under natural rainfall and in the laboratory.

2. Study site

The Houay Pano catchment, located 10 km south of Luang Prabang in northern Laos (Fig. 1), has been part of the MSEC (Monitoring Soil Erosion Consortium) network since 1998 (Valentin et al., 2008). The tropical monsoon climate of the region is characterized by the succession of dry and wet seasons with *ca.* 80% of rainfall occurring during the rainy season from May to October (Ribolzi et al., 2008). The Houay Pano stream has an average base flow of 0.4 ± 0.1 L s^{-1} and is equipped with 2 gauging stations that subdivide the catchment into nested subcatchments. These stations, S1 and S4, draining 20 ha and 60 ha respectively, are located along the main stem of the stream. Between S1 and S4 stations, water flows through a swamp (0.19 ha), supplied with water by a permanent groundwater table (Fig. 1). Only temporary footslope and flood deposits can be found along this narrow section of the stream and the swamp represents the major sediment accumulation zone in the Houay Pano catchment. The Houay Pano stream flows into the Houay Xon River (22.4 km^2 catchment) and is continuously monitored at S10 (draining a 11.6 km^2 catchment), located 2.8 km downstream of S4. The Houay Xon is a tributary of the Nam Dong River, flowing into the Mekong River within the city of Luang Prabang (Ribolzi et al., 2010).

The geological basement of the Houay Pano catchment is mainly composed of pelites, sandstones and greywackes, overlaid in its uppermost part by Carboniferous to Permian limestone cliffs. Soils consist of deep (>2 m) and moderately deep (>0.5 m) Alfisols (UNESCO, 1974), except along crests and ridges where Inceptisols can be found (Chaplot et al., 2009). Soils have a low cation exchange capacity and a low pH ranging between 4.9 –5.5 across the catchment. Native vegetation consisted of lowland forest dominated by bamboos that were first cleared to implement shifting cultivation of upland rice at the end of the 1960s (Huon et al., 2013). Elevation across the catchment ranges *ca.* 272–1300 m.a.s.l. As cultivation takes place on steep slopes (ranging between 3-150%), the catchment is prone to soil erosion (Chaplot et al., 2005; Ribolzi et al., 2011). Due to the decline of soil productivity triggered by soil erosion over the years (Patin et al., 2012) and to an increasing labour need to control weed invasion (Dupin et al., 2009), farmers progressively replaced rice fields by teak plantations in the catchment (Fig. 1). During the present study, main land uses in the Houay Pano catchment were teak plantations (36% of total area), rotating cropping land (35%), Job's tears (10%), banana plantations (4%) and upland rice fields (3%); the forest covering less than 9% of the area. The land use was different in the larger area drained by S10, with 56% of the surface covered with forests, 15% under teak plantations and 23% under cropland.

[Fig. 1]

3. Materials and methods

3.1. Sample and data collection

Rainfall, stream and overland flow waters were sampled during the May 23 flood in 2012. Rainfall intensity was monitored with an automatic weather station (elevation: 536 m.a.s.l.) and stream discharge was calculated from water level continuous recording and rating curves. Rainfall was sampled with three cumulative collectors, located in the village near the confluence between Houay Pano and Houay Xon streams, near a teak plantation on the hillslopes located just upstream of the village and within the Houay Pano catchment. Overland flow was collected at the outlet of 1-m^2 experimental plots. Stream water was collected in plastic bottles after each 20-mm water level change by automatic samplers installed at each gauging station. Fifty-six total suspended sediment (TSS) samples were collected at the three stations (S1, S4, S10). Samples were dried shortly after collection in an oven (t ≈ 100°C) for 12-48 h. In addition, sediment deposited upstream of S4 in the river channel (top 0-1 cm of in-channel deposits collected using a plastic trowel) was sampled the day before the May 23 flood to document the initial radionuclide activity. Surface soil samples (top 0–5 cm; n=65) were collected using plastic trowels on the hillslopes connected to the Houay Pano Stream and the Houay Xon River (Fig. 1) during three campaigns conducted in July 2002 (Huon et al., 2013), May 2012 and December 2012. Additional gully (n = 6) and riverbank (n = 8) samples were also collected in December 2012 to document the characteristics of the potential subsurface sources of sediment to the river.

Cumulative TSS exports were calculated at each station by summing the TSS masses exported between two successive sample collections. As no rating curve could be determined between TSS and Q (hysteresis patterns) during the entire event (absence of causal relationship between both parameters), TSS concentration was considered to vary linearly between successive measurements. Considering the relatively high number of successive samples collected at each station and the resulting high temporal resolution of TSS measurements, this assumption appeared to be reasonable. Sediment yields were calculated by dividing the cumulative TSS exports by the corresponding sub-catchment area.

3.2. Sample preparation and radionuclide analyses

To reduce the volume of rainwater (0.6 - 18 L) that would have been required to conduct direct gamma spectrometry analyses, fallout radionuclide recovery was performed in the field by co-precipitation with aluminium hydroxides (Ciffroy et al., 2003; Evrard et al., 2010). Samples were prepared by adding 1.5 g of aluminium chloride hexahydrate. Co-precipitation was achieved by addition of 1-N NaOH solution until pH attained 8.5-9.0. After 5 hours, the supernatant was removed and the precipitates were placed in an aluminium tray and dried in an oven. All residues were placed in polypropylene tubes and sealed airtight to contain ^{222}Rn and allow in-growth of its decay products. Counting was conducted at the Laboratoire des Sciences du Climat et de l'Environnement (LSCE) in Gif-sur-Yvette by gamma spectrometry using a low-background, high-efficiency, well-type Ge detector with a crystal volume of 220 cm^3 (GWL-220-15 Ortec®). Most samples were analysed within less than 53 days (^{7}Be half-life) following the rainfall event.

Radionuclide activities were measured in a total of 45 individual or composite (depending on the quantity of material recovered) suspended sediment samples (0.2 – 15.1 g), 1 riverbed sediment sample (72 g) and 29 soil samples (48 – 78 g). Samples were packed into 15-60-ml (depending on the quantity available) polyethylene specimen cups and sealed airtight. The ^{7}Be, ^{137}Cs and ^{210}Pb activities were determined at 477.6 keV, 661.6 keV and 46.5 keV, respectively, by gamma spectrometry using the very low-background coaxial N- and P- type GeHP detectors (Canberra® and Ortec®) at LSCE. ^{210}Pb$_{xs}$, was calculated by subtracting the supported activity from the total ^{210}Pb activity (measured at 46.5 keV) using two ^{226}Ra daughters, i.e. ^{214}Pb (average count at 295.2 and 351.9 keV) and ^{214}Bi (609.3 keV). When insufficient matter was available (<5 g), counting was performed with the same well-type Ge detector as for rainfall analyses. All measurements were corrected for background level determined every two months as well as for detector and geometry efficiencies. All results were expressed in Bq kg^{-1}. Activities were also decay corrected to the sampling date. Counting time reached a maximum of *ca.* 13 x 10^4 s for rainwater samples and *ca.* 25 x 10^4 s for soil and sediment samples, to optimize counting statistics. Counting efficiencies and reliability were conducted using internal and certified International Atomic Energy Agency (IAEA) standards prepared in the same specimen cups as the samples. Efficiencies were interpolated for ^{7}Be energy. Uncertainties on radionuclides activities were *ca.* 10% for ^{210}Pb$_{xs}$, 20% for ^{7}Be and up to 30% for ^{137}Cs.

3.3. Estimates of fresh sediment (F) and surface soil (α) contributions to suspended loads

Respective proportions of (1) fresh sediment vs. particles isolated from recent fallout and, (2) surface soil -derived particles and subsurface particles (mobilized from gullies and riverbanks) were estimated in TSS load. The fresh sediment proportion in TSS load was estimated following the method (Eq. 1) proposed by Matisoff et al. (2005):

$$F = 100 \times [(A/B) / (A_0/B_0)] \quad (1)$$

where F is the percentage of fresh sediment, A and B are the ^{7}Be and $^{210}Pb_{xs}$ activities in suspended sediment (Bq kg^{-1}) and A_0 and B_0 are the ^{7}Be and ^{210}Pb activities in rainfall (Bq l^{-1}). Although the spatio-temporal variability of ^{7}Be and ^{210}Pb wet deposition may be important for longer events or for successive storms, this study focused on a single event of short duration and the use of a single value to characterize $^{7}Be/^{210}Pb$ in rainfall was shown to be meaningful (Gourdin et al., 2014).

Proportion of surface soil -derived particles in a given sediment sample was estimated with Eq. 2 (e.g., Brigham et al., 2001; Olley et al., 2012):

$$\alpha = 100 \times [\,(Cs_{sample} - Cs_{subsurf.}) / (Cs_{surf.soil} - Cs_{subsurf.})\,] \quad (2)$$

where α is the percentage of particles derived from surface soil, Cs_{sample} is the ^{137}Cs activity in the sample, $Cs_{subsurf.}$ is the mean ^{137}Cs activity in the subsurface soils and $Cs_{surf.soil}$ is the mean ^{137}Cs activity in the surface soils (top 0-2 cm).

3.4. Checking the field recovery procedure and the assumptions underpinning the ^{7}Be method

In order to determine the efficiency and reproducibility of radionuclide recovery by co-precipitation, experiments were carried out at LSCE. Six aliquots (2 L each) of rainwater were prepared by adding aluminium chloride hexahydrate. Three of them were completely evaporated using heating plates at 150°C for two days, assuming that 100% yields are obtained by total evaporation (Cazala et al., 2003). Co-precipitation was conducted on the three other aliquots using the procedure described in section 3.2. Supernatants were also evaporated to determine the residual radionuclide activity that might still be present in the solution after precipitation.

A simple experiment was carried out to assess ^{7}Be adsorption kinetics on soil particles during rainfall. Five aliquots of a composite topsoil sample collected in the Houay Pano catchment in Laos were mixed with rainwater (4.4 g L^{-1}) and centrifuged at high velocity (25,000 rpm, *ca.* 78650 x g) using the Beckman Coulter® J-26 XP air-cooled centrifuge facility at UMR Bioemco. The total contact time between soil particles and rainwater, including acceleration and deceleration phases of the centrifuge, were 13, 23, 31, 41 and 72 min. After removal of supernatants, recovered sediments were evaporated and analysed by gamma spectrometry as described in section 3.2.

In order to check the underlying assumption that fresh sediment labelling is characterized by a $^{7}Be/^{210}Pb_{xs}$ similar to that of rainwater, ratios were compared in both rainfall and overland flow water. To this end, overland flow and rainfall samples were collected simultaneously at the outlet of a 1-m^2 experimental plot and of a *ca.* 8-m^2 rain-collector during the June 1 rainfall event at the field site. The experiment was conducted on a fallow soil with 33% slope and 60% vegetation cover (*ca.* 10 cm high). The rain collector was installed at 1.8 m height from the soil surface to avoid splash contamination. Rainwater and overland flow samples were collected in plastic bottles at the outlet of the plot and of the rain collector. Radionuclide activities were determined in TSS samples dried in an oven, and radionuclide recovery of rainfall samples was realized by co-precipitation as described in section 3.2. Radionuclide stock variations for the experimental plot were calculated with 1 min- steps during the event using Eq. 3:

$$\Delta S_t = I_t - E_t \qquad (3)$$

Where ΔS_t is the stock variation of the plot, I_t is the amount of radionuclide supplied by rainfall to the plot and E_t is the amount of radionuclide exported from the plot by overland flow, between time t-1 and time t (expressed in Bq m^{-2}).

3.5. Particle size distribution measurements

Particle size distribution (PSD) was analysed after a 48-h rehydration of TSS samples (≈1 g) in 50 mL of distilled water, followed by a 5-min immersion in a Branson 2510 ultrasonic cleaning bath. We used the laser diffraction system (Malvern® Mastersizer 2000) coupled to a liquid dispersing unit (Hydro 2000G) both available at the Earth Science Department (University Paris-Sud, Orsay, France). As sediment samples were dried and rehydrated, these PSD do not correspond to the "effective" PSD (Jouon et al., 2008). However, as no dispersing agent was used, the distributions provided here also differ from "absolute" PSD. The protocol was adjusted in order to ensure particle suspension without breaking all the aggregates and allowing flocs' formation in the presence of organic matter, which is assumed to occur naturally in the stream. Replicate measurements were realized to check reproducibility (*ca.* ±0.5 µm), and the timing of analysis was adapted to optimize signal stability. The PSD of each sample was obtained for 100 grain size classes ranging between 0.02 and 2000 µm. The parameter chosen for comparison between the particle size distributions is d_{50}, corresponding to the median diameter of sediment particles (expressed in µm) with 50% of total volume of particles in the sample below this grain size (e.g. Jouon et al., 2008; Grangeon et al., 2012).

3.6. Water electrical conductivity measurement

In order to characterize stream / river baseflow dilution by storm event water, water electrical conductivity was monitored every 6-min at the inlet of each gauging station using Schlumberger in situ CTD probes, and additional measurements were conducted using an YSI® 556 probe on each collected sample.

4. Results

4.1. Checking methodological assumptions

4.1.1. Radionuclide recovery procedure

Reproducibility and efficiency of fallout radionuclide recovery procedures used in this study are presented for ^{7}Be. Reproducibility was slightly better when conducting the total evaporation procedure (as described in Cazala et al., 2003), with a deviation of *ca.* 0.5% between triplicates, than when achieving co-precipitation (5% deviation). Differences induced by both treatments were lower than the 10% analytical uncertainty associated with ^{7}Be activities measured by gamma spectrometry. The recovery was equivalent for both co-precipitation (90 ± 6 mBq L^{-1}) and evaporation (86 ± 6 mBq L^{-1}) procedures. Activities measured in the supernatant (co-precipitation procedure) remained below the lower instrumental detection limits (<3% of co-precipitated sample activity) and a *ca.* 100% recovery of fallout radionuclides can therefore be assumed.

4.1.2. Fallout radionuclide adsorption kinetics

The adsorption kinetics experiment did not show any significant variation in ^{7}Be and $^{210}Pb_{xs}$ activity with time. The ^{7}Be activity in rainwater used in the experiment was 15 ± 2 Bq kg^{-1} and the initial ^{7}Be activity was null for soil particles. Mean activities of 10 ± 3 Bq kg^{-1} (range: 7 ± 2 to 13 ± 3 Bq kg^{-1}) for ^{7}Be and 29 ± 3 Bq kg^{-1} (range: 25 ± 4 to 32 ± 4 Bq kg^{-1}) for $^{210}Pb_{xs}$ were determined in particles. Taking into account all analytical uncertainties, total rainwater ^{7}Be adsorption was fulfilled at *ca.* 75-100% for all samples. The supply of $^{210}Pb_{xs}$ by rainfall (2.0 ± 0.2 Bq kg^{-1}) was low compared to its initial content in the soil (26 ± 2 Bq kg^{-1}). However, the activity in $^{210}Pb_{xs}$ measured in the soil after the experiment (28 ± 2 Bq kg^{-1}) remained consistent with the occurrence of additional sorption. Furthermore, ^{7}Be- and $^{210}Pb_{xs}$- sorption by soil particles occurred in less than 13 min, corresponding to the shortest contact time between water and soil particles that could be achieved during the experiment.

^{7}Be and ^{210}Pb$_{xs}$ labelling of soil particles by rainfall occurred very quickly as shown in other studies (e.g. Taylor et al., 2012).

4.1.3. Fresh sediment labelling by rainfall

During the 1-m² plot experiment conducted on June 1, a 45 min- storm event with 11-mm cumulative rainfall occurred. It triggered the export of 8.5 L of overland flow and 20 g of fresh sediment. TSS samples (n = 13) were mixed together to form 3 successive composite samples. Rainfall was characterised by activities ranging 57 - 171 ± 30 mBq L^{-1} for ^{7}Be and 37 - 166 ± 30 mBq L^{-1} for ^{210}Pb$_{xs}$. Initial activities in surface soil (5 upper mm) collected on May 31 before rainfall were 8 ± 1 Bq kg^{-1} for ^{7}Be and 60 ± 2 Bq kg^{-1} for ^{210}Pb$_{xs}$. Overland flow collected during rainfall displayed activities ranging 31 - 219 mBq L^{-1} for ^{7}Be and 11 - 345 mBq L^{-1} for ^{210}Pb$_{xs}$. Related activities in suspended sediments ranged 24 - 95 ± 10 Bq kg^{-1} for ^{7}Be and 10 - 100 ± 10 Bq kg^{-1} for ^{210}Pb$_{xs}$. By comparison of radionuclide inputs and exports (expressed in Bq m^{-2} min^{-1}) from the experimental plot, stocks of radionuclides were calculated for each time step using Eq. 3. The evolutions of these stocks during each of the 45 minutes of the event are plotted versus the TSS concentration in the corresponding overland flow exported from the experimental plot on Fig. 2.

[Fig. 2]

Stock variations were correlated with TSS concentration for ^{7}Be (r^2 = 0.75; Fig. 2a), ^{210}Pb$_{xs}$ (r^2 = 0.89; Fig. 2b) and ^{137}Cs (r^2 = 0.88; Fig. 2c), confirming that radionuclides were adsorbed by particles. Rainfall ^{7}Be and ^{210}Pb$_{xs}$ inputs compensated the exports by TSS loads below 2 g L^{-1} in the overland flow.Rainwater brought a total amount of 1.02 Bq m^{-2} for ^{7}Be and 1.01 Bq m^{-2} for ^{210}Pb$_{xs}$ (ratio: 1.0 ± 0.2). In the same time, overland flow exported 1.30 Bq m^{-2} for ^{7}Be and 1.59 Bq m^{-2} for ^{210}Pb$_{xs}$ (ratio: 0.8 ± 0.2). Comparing total cumulative inputs and exports, stock depletions were -0.27 Bq m^{-2}, -0.59 Bq m^{-2} and -0.02 Bq m^{-2} during the event for ^{7}Be, ^{210}Pb$_{xs}$ and ^{137}Cs, respectively. However, as no soil sample was collected after the event, control of the stock balance could not be achieved. Overland flow particles F were estimated to 81 ± 20%, consistent with the assumption that freshly labelled sediments have $^{7}Be/^{210}Pb_{xs}$ similar to rainfall. Taking into account analytical errors associated with gamma - counting and their impact on $^{7}Be/^{210}Pb_{xs}$ estimates, this result strengthens the reliability of this ratio to fingerprint fresh sediment supply at the onset of the rainy season.

4.2. Application of the tracing method to a flood

4.2.1. Composition of potential sediment sources within the catchment

Mean radionuclide characteristics of surface soils, gullies and stream banks materials collected in the catchment are reported in Table 1.

[Table 1]

Surface and subsurface (stream banks and gullies) sources were best discriminated by their ^{137}Cs activity that is higher in surface soils. Mann-Whitney *U*-tests indicate statistically significant differences between surface and subsurface sources samples at $p<0.001$ for both ^{137}Cs and $^{210}Pb_{xs}$ activities.

4.2.2. Hydro-sedimentary characteristics of the May 23 flood

The particles exported during a flood at the onset of the rainy season 2012 in the Houay Xon catchment were collected successively all along the event at nested stations (Fig. 1) and analysed to investigate their sources and dynamics. The main characteristics of this event are described thereafter. The studied flood was triggered by a storm that occurred on May 23 2012 between 11:36 am and 12:24 pm. Rainfall intensity reached 85 mm h^{-1} between 11:54 am and 12:00 am, and cumulated 27 mm rainfall in 48 min. This event was below 0.01 y return period value (34.7 mm daily rainfall), according to Bricquet et al. (2003) for the 1950-2000 period. It was the first significant erosive event of the rainy season and the first event with rainfall intensity exceeding 80 mm h^{-1}. Rainfall samples collected during the event displayed ^{7}Be activities ranging between 110 – 330 mBq L^{-1}. The main hydro-sedimentary characteristics of the flood are reported for the three gauging stations in Fig. 3-4-5.

[Fig. 3-4-5]

The lag time between stream discharge (Q) and rainfall intensity peaks differed at each station. Q increased 10 min after the rainfall peak and reached its maximum 10 min later at S1 (Fig. 3a), whereas at S4, Q rise started during the rainfall peak, and the Q peak occurred *ca.* 15 min later (Fig. 4a), i.e. 5 min before S1. This behaviour suggests an earlier beginning of rainfall on hillslopes located upstream of S4, with a progressive displacement of raincloud toward the location of the automatic weather station and the upstream S1 draining area (Fig. 1). Downstream at S10, the lag time between rainfall and Q peaks increased to 70 min (Fig. 5a). The evolution of TSS concentration as a function of stream discharge (Fig. 3b-4b-5b) displayed counterclockwise hysteresis dynamics (Williams, 1989) in the three subcatchments. Even though Q increased faster than TSS concentration at the beginning of the flood, water EC decreased concomitantly in the three stations (Fig. 3c-4c-5c). This evolution of stream EC suggests the progressive mixing of highly mineralized pre-event water (PEW, i.e. groundwater - high EC) with a low TSS concentration by weakly mineralized event water (EW, i.e. overland flow - low EC) with high sediment loads, the proportion of the EW increasing with decreasing EC (e.g., Nakamura, 1971; Pilgrim et al., 1979; Sklash and Farvolden, 1979; Ribolzi et al., 1997; Collins and Neal, 1998). Despite relatively common TSS-Q trends, major differences between the three stations were observed. At S1 the TSS maximum occurred 10 minutes after the water discharge peak and differed markedly between the water rising and recessing stages. During a second stage, TSS increased rapidly at the onset of Q decrease, reflecting the contribution of overland flow loaded with sediments originating from remote areas of the subcatchment.

During a third stage, TSS and Q decreased together. Station S4 showed the fastest response to rainfall. In contrast to S1, S4 displayed three discharge peaks. The first (and main) one likely corresponds to the contribution, upstream of the station, of hillslopes relatively close and well connected to the stream channel. The second and/or third peaks rather result from later arrival (at 12:55) of water flow originating from remote parts of the catchment (possibly including that exported from S1 30 min before). The evolution of Q *vs.* TSS during the rising and falling water stages followed relatively similar pathways (Fig. 4b). At S10, downstream of S4, Q increased with a time-lag of 22 min after the rainfall peak and the maximum Q was reached 45 min later. Two main successive water discharge peaks (12:42 and 13:17) were related to three successive TSS peaks (13:07, 13:33, 13:57; Fig. 5a), reflecting contributions to the river from distinct parts of the catchment. Each of the two first TSS peaks occurred *ca.* 30 min after the related Q peak. The first TSS peak (24 g L^{-1}) was recorded just before the second Q peak whereas the second and the third TSS peaks (respectively 25 and 22 g L^{-1}) occurred during the recessing stage, 22 and 27 min later.

Overall, high TSS concentrations (> 5 g L^{-1}) were maintained during the recession phase at the three monitoring stations. The amounts of sediment (calculated as described in section 3.1) exported from the three subcatchments are summarized in Table 2.

[Table 2]

Unfortunately, no sample was collected at the highest Q at S1. Therefore, these sediment exports and yields estimates (Table 2) could be slightly underestimated. The highest sediment yield was calculated at S4. It might be related to the larger area covered by teak plantations sensitive to soil erosion (32%) in this subcatchment, that is two-fold higher than in the drainage areas of S1 (14%) and S10 (15%). The river channel morphology and the hillslope-to-river connectivity varied across the area, as mentioned above in the description of hydro-sedimentary characteristics. The higher connectivity between cultivated hillslopes and the river upstream of S4 might also explain the higher sediment yield from this station.

4.2.3. Radionuclide measurements and estimates of fresh sediment (F) and surface-derived particle (α) contributions

Rainfall activities ranged 0.11-0.33 Bq L^{-1} and 0.04-0.12 Bq L^{-1} for ^{7}Be and $^{210}Pb_{xs}$ respectively, with a mean $^{7}Be/^{210}Pb_{xs}$ of *ca*. 2.8. Weight fractions of fresh sediment were calculated for all TSS samples using this latter value. As expected, ^{137}Cs was not detected in rainfall. No ^{7}Be activity (<3 Bq kg^{-1}) could be determined for the deposited sediment sample collected just before the flood (May 22) upstream S4 confirming the almost complete decay of the previous year fallout.

At S1 and S4, ^{137}Cs activity in TSS increased with water discharge from *ca.* 1.0 Bq kg^{-1} during the rising stage, then peaked near its maximum level (1.5-2.0 Bq kg^{-1}) and remained nearly constant (*ca.* 1.5 ± 0.6 Bq kg^{-1}) during the falling stage period (Fig. 3e-4e). The evolution was more variable at S10 (Fig. 5e). During the beginning of the rising stage, ^{137}Cs activity in TSS was rather stable (*ca.* 0.8 ± 0.2 Bq kg^{-1}) with intermediate values between surface soil signature and ^{137}Cs-depleted particles, found in gullies and stream banks (Table 1). In contrast, $^{210}Pb_{xs}$ activities measured at S1, S4 and S10 (Fig. 3f-4f-5f) were generally higher than the average level measured in catchment soils (*ca.* 40 Bq kg^{-1}, Table 1), in particular during the rising stage of the flood at S4. This little enrichment may result from the preferential export of fine-grained particles – enriched in fallout radionuclides – by overland flow (e.g., Walling and He, 1999; Matisoff, 2014). However, the values found in TSS remained in the range of bulk surface soils $^{210}Pb_{xs}$ activities (up to 106 ± 3 Bq kg^{-1}). Contrary to ^{137}Cs, ^{7}Be activities (and corresponding $^{7}Be/^{210}Pb_{xs}$) were higher during the rising stage and then started to drop at peak flow maximum (Fig. 3g-4g-5g), following a dilution pattern consistent with the behaviour of water EC (Fig. 3c-4c-5c). The overall trend in S10 consisted in the mixing of: (i) particles with low ^{137}Cs activities – originating from subsurface sources like collapsed riverbanks or deep rills / gully floor erosion (Hancock et al., 2014) – but tagged with ^{7}Be and $^{210}Pb_{xs}$ supplied by recent rainfall and (ii) sediments initially originating from surface soils with high ^{137}Cs but low ^{7}Be activities (which suggests that they were immersed under water in deposition areas such as in swamps – see Huon et al., 2013 – and isolated from recent fallout labelling before being resuspended during the investigated flood).

A F value of *ca.* 10-30% was estimated during flood peaks and falling water stages (Fig. 3h-4h-5h). Values in $^{7}Be/^{210}Pb_{xs}$ were not significantly different in most samples, except during the beginning of the flood rise in S10, resulting in higher F (Fig. 5h). Those large analytical uncertainties were either due to low sediment yields or to the short gamma counting time to allow for analysing the entire sample set. However, proportional calculations show that mixing of (1) 20-25% of fresh sediment originating from stream banks, depleted in ^{137}Cs (*ca.* 0.4 Bq kg^{-1}, Table I), with (2) 75-80% of ^{137}Cs- labelled surface soil particles (*ca.* 2.2 Bq kg^{-1}, Table I), would provide estimates of *ca.* 1.8 Bq kg^{-1}, consistent with the ^{137}Cs activities measured in TSS at S1 and S4 (Fig. 3e-4e). The contribution of fresh sediment was more important at S10, up to *ca.* 35% at the beginning of the flood (20% of TSS export during the flood). At S1 and S4, ^{7}Be activities (in Bq L^{-1}) were positively correlated with TSS concentrations ($r^2 = 0.85$ and 0.88, respectively; Fig. 6a-6b) during the entire flood. This behaviour confirms that ^{7}Be is transported by the solid phase in the stream samples of the Houay Pano upstream catchment. However, for S10, no clear trend was observed on a similar plot (not shown). Furthermore, ^{7}Be activities in TSS (in Bq kg^{-1}; Fig. 5g) decrease when TSS loads increase (Fig. 5a). This trend reflects that particles tagged with ^{7}Be that are exported from S10 at the beginning of the flood are then diluted by ^{7}Be-depleted TSS loads, which highlights a different behaviour in the downstream part of the Houay Xon catchment compared with upstream stations of the Houay Pano subcatchment.

[Fig. 6]

Results obtained at S10 suggest a mixing between a ^{7}Be-labelled source of fresh sediment and remobilized sediment from the river channel. In addition, variations in the origin of suspended sediment were observed at this station. Mean ^{137}Cs activity measured at S10 (*ca.* 1.0 Bq kg^{-1}) was lower than at S1 (1.4 Bq kg^{-1}) and S4 (1.6 Bq kg^{-1}), revealing a larger contribution of particles originating from subsurface sources at this station, which is consistent with our field observations. Vegetated riverbanks are less sensitive to erosion upstream of S4 where the stream bed does not deeply incise the bedrock. Using Eq. 2 (section 3.3), we estimated a contribution of *ca.* 90% of ^{137}Cs-depleted sediment at the beginning of the flood at S10. A potential explanation would be that those particles were initially supplied to the river by stream bank erosion or collapse during the former wet season(s). At the end of the previous rainy season, i.e. 6 months before the studied flood, this sediment was deposited in the river channel. As the river level decreased during the dry season, subsequent exposure to atmospheric fallout took place at the beginning of the wet season. The morphology of the riverbed upstream of S10 is consistent with the formation of such deposits. The remainder of sediments depleted in both ^{137}Cs and ^{7}Be were likely "older" particles originating from riverbanks or gullies and deposited in the river channel during the previous years. Furthermore, when plotting estimated F and α for S10, nearly all data points (except 2) are aligned (Fig. 6c). The two outlying samples correspond to the first and the third TSS peaks, which are likely associated with the export of material with a different origin, suggesting the contribution of a third type of source. Both samples are located below the regression line, reflecting their depletion in fallout radionuclides, which suggests that they were supplied by deep gully walls or riverbank erosion processes (Olley et al., 1993, 2012; Hancock et al., 2014) that were not dominant during the rest of the event. When excluding those two samples implying this third secondary source, a negative linear correlation (r^2=0.97; Fig. 6c) is observed during the flood. High contributions of fresh sediment are associated with exports of particles originating from subsurface soils, whereas remobilized sediments are mainly originating from surface soils. This observation outlines the existence of a source of fresh sediment, derived from collapsed riverbanks, that represents a significant proportion of the TSS load conveyed at this station.

4.2.4. Particle size distribution of suspended sediments

The relationship between TSS grain size and water discharge was investigated by comparing d_{50} (median particle size) values for the three stations (Fig. 3d-4d-5d). The lowest d_{50} value (4 µm) was recorded at S4 at the end of the flood whereas, the highest value (12 µm) was measured during the discharge maximum at S10. Mean d_{50} at S1, S4 and S10 reached 6.3, 6.9 and 8.1 µm, respectively, reflecting the increasing discharge and the higher competence of the river in downstream direction.

All three stations presented high d_{50} during the peaks of discharge that corresponded to the transport of both freshly eroded and remobilized particles. During the recessing stage of the flood, transport was progressively replaced by deposition of particles on the streambed, as d_{50} decreased to 5, 5.5 and 6 µm at S1, S4 and S10 respectively.

5. Discussion

5.1. Sediment sources and dynamics along the river continuum

The time-lag between water and sediment peaks observed at S10 may result from the presence of a dense vegetation cover on both riverbed and banks that represent obstacles to flow propagation (Gurnell, 2007). Although it did not stop completely the transport of upstream particles as the discharge was high, it may have slowed them down and delayed their arrival compared to water flow propagation, by increasing Houay Xon River channel hydraulic roughness (Manning, 1889) in a similar way as the so-called “grassed waterways” (GWW) installed in agricultural lands to combat muddy runoff generated on cultivated hillslopes (Evrard et al., 2008). Furthermore, this effect should increase with the distance of transportation (Heidel, 1956) as S4 sediment exports had to travel approximately 3 km before reaching S10. As reported by Williams (1989), such counterclockwise hysteresis dynamics may occur in highly erodible catchments submitted to prolonged erosion. Similar lagging sediment peaks were also observed in larger catchments receiving the successive contributions from areas characterized by low and high specific sediment yields (Yun-Liang et al., 1985). Inversely, Whiting et al. (2005) reported clockwise hysteresis dynamics for suspended sediment concentration and fallout radionuclide activity (in Bq L^{-1}) recorded at successive stations along the Yellowstone River (samples collected during seven different floods between April and July 2000). Smith and Dragovitch (2009) reported several counterclockwise hysteresis events at the upstream station of nested catchments affected by severe gully and riverbank erosion in south-eastern Australia's uplands. However, clockwise hysteresis patterns were mostly observed in these catchments, and they were interpreted as resulting from sediment exhaustion effects, particularly during multi-rise events.

[Fig. 7]

The changes in suspended sediment signatures during the flood at the upstream stations (S1 and S4; Fig. 7a-b) indicate that they were mostly derived from surface soils (tagged by 20th century ^{137}Cs fallout), which is consistent with previous observations made in the Houay Pano catchment (Huon et al., 2013). Previous works by Chaplot et al. (2005) reported the formation of gullies and rills on hillslopes upstream of S4 and S1 in 2001. However, most of those linear features formed during a rainfall event of higher intensity (90 mm cumulative rainfall; return period > 2 yrs). This storm took place in August, i.e. at the period of the rainy season with the lowest infiltrability and highest mean monthly rainfall (Patin et al., 2012). During the 23 May 2012 event, no active gully was observed in the field. Furthermore, we could not quantify specifically the contribution of rill erosion to sediment exports for this event (Evrard et al., 2010; Ben Slimane et al., 2013). Nevertheless, suspended material conveyed at the downstream station contained lower ^{137}Cs activities (Fig. 5e), suggesting a switch in the source of particles at this scale with the likely contribution of collapsed riverbanks (e.g. Nagle and Ritchie, 2004). Decreasing ^{137}Cs fluxes with increasing drainage areas had been previously reported by Whiting et al. (2005) and interpreted as resulting from bank erosion increase in downstream direction. These authors also reported the dominance of new sediment at upstream stations and early in the hydrograph. Indeed, the global trend observed at S10 (Fig. 7c) corresponded to the arrival, at the beginning of the flood, of particles from collapsed riverbanks originating from the Houay Xon River channel section, associated with a first peak of discharge. Then, during the main discharge peak, more particles mobilized from remote surface soils by overland flow were exported. Those materials were mixed with remobilized sediment from the river channel that diluted the fresh sediment input signal. Finally, as Q decreased, remobilized and eroded particles from most remote sources were exported and progressively deposited.

Cumulative exports of fresh sediment were estimated to *ca.* 0.3, 3 and 26 Mg for S1, S4 and S10, respectively. They represented respectively *ca.* 13, 12 and 20% of the total suspended sediment exports previously estimated (see section 4.2.2; Table 2). Corresponding estimates in individual suspended sediment samples ranged *ca.* 10 - 60% of surface soil-derived particles. Furthermore, the mean contribution of surface-derived particles was estimated to *ca.* 60 and 76% at S1 and S4, respectively, whereas it amounted to only 29% at S10, reflecting the importance of subsurface sources contribution downstream of S4 (Fig. 7).

5.2. Methodological assumptions and prospects

Due to the absence of pre-event ^{7}Be labelling (Appendix) the May 23 flood event appeared to be the first major erosive flood of the 2012 rainy season. Therefore, the hypotheses underpinning the use of the ^{7}Be/^{210}Pb$_{xs}$ method (Matisoff et al., 2005; Schuller et al., 2006) were simplified. At the plot scale, ^{7}Be/^{210}Pb$_{xs}$ in rainwater and fresh sediment showed a strong similarity during a comparable storm to that of May 23. As this study focused on a single event of short duration (*ca.* 1h rainfall with 60% total cumulative water depth in 12 min) the use of a single integrated value for rainfall ^{7}Be/^{210}Pb$_{xs}$ proved to be meaningful. However, for longer lasting events, progressive decrease of radionuclide content in rainwater may occur (Wallbrink and Murray, 1994; Ioannidou and Papastefanou, 2006; Gourdin et al., 2014). In order to estimate radionuclide signature of fresh sediment inputs to the rivers, overland flow could be collected and analysed instead of rainfall. Indeed, as showed by Chaplot and Poesen (2012), only a limited proportion of soil-detached (and freshly ^{7}Be-labelled) particles may reach the Houay Pano stream channel and be transported downstream. The transport of those particles by overland flow progressively decreased with rainfall intensity and most of mobilized materials were deposited and remained on hillslopes. Comparable conclusions could be drawn from soil ^{137}Cs inventories (Huon et al., 2013). This behavior may be responsible for the global trend to progressive decrease of ^{7}Be activity in TSS observed at all stations during the event.

Studies investigating ^{7}Be/^{210}Pb$_{xs}$ variations in catchments and rivers grew in number during the last years (Taylor et al., 2013). However, they were conducted over a wide range of time (1h–1yr) and spatial scales (0.7–390 km^2) for different environmental and climatic contexts, and their results may not be easy to compare to our study. The main ^{7}Be/^{210}Pb$_{xs}$ values and related F estimates found in the literature are summarized in Table 3.

[Table 3]

A large seasonal variability was observed for these ratios depending, among other factors, on the origin of air masses evolving throughout the year and across regions (Bourcier et al., 2011). We could, nevertheless, compare our results with those obtained for a composite sediment sample collected during the first erosive flood of the rainy season in central Mexico (Evrard et al., 2010) where similar conditions prevailed. A comparable contribution of fresh sediment (*ca.* 25 ± 4%) was supplied to the stream, suggesting the dominance (75–87%) of processes remobilizing “older” material at the beginning of the wet season. However in both cases, more detailed spatial information is needed to characterize the origin (surface vs. subsurface) of both freshly eroded and remobilized sediment. In this study, we could determine the sources supplying suspended sediment (mainly derived from surface soils) during this early monsoon event and constrain their dynamics. The bulk of exported particles was remobilized from previous year deposits accumulated in the stream/river channel system.

The chosen nested approach provided a way to outline changes in the succession of dominant processes along the river system, from headwaters to the outlet with contrasting sensitivities to erosion along the stream path (Table 2) and a variable connectivity between hillslopes and the main river channel. Whilst hillslopes were directly connected to the stream in upper parts of the catchment, the connection between surface sources and the Houay Xon River was less direct in the downstream sections, characterized by a gentler topography and the presence of depositional areas including a swamp and a wider river channel. Furthermore, the variations in land uses and covers characterized by varying sensitivities to erosion observed across the catchment also partly explain the differences in sediment yields calculated in the drainage areas of the 3 stations. The higher sediment yields calculated at S4 might therefore be explained by the presence of well-connected hillslopes covered by teak plantations. Indeed, this particular land use has been detected as generating large quantities of runoff, especially when teak age exceeds 10 years (Patin et al., 2012).

Our results suggest that information on sediment sources (i.e., surface vs. subsurface) should be systematically provided when using $^{7}Be/^{210}Pb_{xs}$ to avoid misinterpretations on their variations. Furthermore, given the rather large uncertainties associated with their results due to logistical and analytical constrains that are difficult to reduce, interpretation of these ratios should remain cautious (e.g. by mentioning proportions of fresh sediment instead of sediment ages in days). It should also focus on the identification of sources and processes of sediment export during the main flood stages. Under those conditions, the $^{7}Be/^{210}Pb_{xs}$ method will provide useful constrains on the processes controlling sediment dynamics in rivers and support design and implementation of efficient soil conservation measures to limit erosion.

6. Conclusions

An early monsoon flood was monitored at three nested stations in the Houay Xon catchment (Laos) and suspended sediment content in fallout radionuclides was analysed throughout the event. Our results showed that rainwater fallout radionuclides were quickly (< 13 min) bound to surface soil particles. Furthermore, freshly mobilized sediments in overland flow displayed a $^{7}Be/^{210}Pb_{xs}$ similar to the one measured in rainwater.

Consequently, fresh sediment contributions were estimated for each of the three nested sub-catchments. During this first erosive flood of the rainy season, remobilized particles represented the main type of sediment exported, whatever the spatial scale considered. Contribution of sediments originating from surface soils was dominant upstream (69-78%) whereas they only represented 36% of suspended load downstream, highlighting the key role played by land use and hill slope connectivity on sediment delivery to the river in the different subcatchments.

Furthermore, fallout radionuclides provided a mean to identify the contribution of ^{7}Be-labelled particles originating from collapsed riverbank sediments, deposited on aerial exposed areas in the river channel.

This study highlights the interest of combining $^{7}Be/^{210}Pb_{xs}$ measurements with additional parameters providing information on sediment origin in order to avoid misinterpretation of their dynamics. Further work should attempt to use similar combinations of tracers applied to a longer river continuum (integrating more or larger nested subcatchments). Tracking the downstream flood propagation would provide an opportunity to outline the evolution of dominant processes and sources in larger mountainous tropical catchments where excessive erosion results in critical problems. Providing such information appears crucial to design efficient conservation measures in upstream catchments to prevent an excessive supply of sediment to the rivers.

Acknowledgements

The authors would like to thank the Lao NAFRI (National Agriculture and Forestry Research Institute in Vientiane) and the MSEC project (Multi-Scale Environment Changes) for their support. They are also grateful to Keo Oudone Latsachack, Bounsamai Soulileuth and Chanthamousone Thammahacksa for their kind, constant and irreplaceable help in the field and to Christophe Colin and Olivier Dufaure for their help to organize and conduct the Particle Size Distribution measurements. Elian Gourdin received a PhD fellowship from Paris-Sud University. This work received financial support from the French CNRS EC2CO / BIOHEFECT programme (Belcrue project). Finally, the authors would like to thank the three anonymous reviewers, whose comments helped to improve the manuscript.

7. References

Ben Slimane, A., Raclot, D., Evrard, O., Sanaa, M., Lefèvre, I., Ahmadi, M., Tounsi, M., Rumpel, C., Ben Mammou, A., Le Bissonnais, Y. (2013). Fingerprinting sediment sources in the outlet reservoir of a hilly cultivated catchment in Tunisia. *Journal of Soils and Sediments*, 13(4), 801–815.

Bonniwell, E. C., Matisoff, G., Whiting, P. J. (1999). Determining the times and distances of particle transit in a mountain stream using fallout radionuclides. *Geomorphology*, 27, 75–92.

Bourcier, L., Masson, O., Laj, P., Pichon, J. M., Paulat, P., Freney, E., Sellegri, K. (2011). Comparative trends and seasonal variation of ^{7}Be, ^{210}Pb and ^{137}Cs at two altitude sites in the central part of France. *Journal of Environmental Radioactivity*, 102(3), 294–301.

Bricquet, J.-P., Boonsaner, A., Bouahom, B., Toan, T. D. (2003). Statistical Analysis of Long Series Rainfall Data: A Regional Study in South-East Asia. In A. R. Maglinao, C. Valentin, F. Penning de Vries (Eds.), *From soil research to land and water management: harmonizing people and nature: proceedings of the IWMI-ADB project annual meeting and 7th MSEC assembly. Vientiane (LAO).* (pp. 83–89). Vientiane (LAO): IWMI-ADB Project Annual Meeting; MSEC Assembly, 7.

Brigham, M.E., McCullough, C.J., Wilkinson, P. (2001). Analysis of suspended-sediment concentrations and radioisotope levels in the Wild River Basin, Northwest Minnesota, 1973–98. *U.S. Geological Survey Water- Resources Investigations Report 01-4192*, 21 p.

Cazala, C., Reyss, J. L., Decossas, J. L., Royer, A. (2003). Improvement in the determination of ^{238}U, $^{228-234}$Th, $^{226-228}$Ra, ^{210}Pb, and ^{7}Be by gamma spectrometry on evaporated fresh water samples. *Environmental Science and Technology*, 37(21), 4990–4993.

Chaplot, V, Coadoulebrozec, E., Silvera, N., Valentin, C. (2005). Spatial and temporal assessment of linear erosion in catchments under sloping lands of northern Laos. *Catena*, 63(2-3), 167–184.

Chaplot, V., Podwojewski, P., Phachomphon, K., Valentin, C. (2009). Soil Erosion Impact on Soil Organic Carbon Spatial Variability on Steep Tropical Slopes. *Soil Science Society of America Journal*, 73(3), 769.

Chaplot, V., Poesen, J. (2012). Sediment, soil organic carbon and runoff delivery at various spatial scales. *Catena*, 88(1), 46–56.

Ciffroy, P., Reyss, J. L., Siclet, F. (2003). Determination of the residence time of suspended particles in the turbidity maximum of the Loire estuary by ^{7}Be analysis. *Estuarine, Coastal and Shelf Science*, 57(4), 553–568.

Collins, R.U., Neal, C. (1998). The hydrochemical impacts of terraced agriculture , Nepal. *Science of the Total Environment,* 212, 233–243.

Descroix, L., González Barrios, J. L., Viramontes, D., Poulenard, J., Anaya, E., Esteves, M., Estrada, J. (2008). Gully and sheet erosion on subtropical mountain slopes: Their respective roles and the scale effect. *Catena*, 72(3), 325–339.

Dominik, J., Burrus, D., Vernet, J.-P. (1987). Transport of the environmental radionuclides in an alpine watershed. *Earth and Planetary Science Letters*, 84(2–3), 165–180.

Downing, J. A., Cole, J. J., Middelburg, J. J., Striegl, R. G., Duarte, C. M., Kortelainen, P., Prairie, Y. T., Laube, K. A. (2008). Sediment organic carbon burial in agriculturally eutrophic impoundments over the last century. *Global Biogeochemical Cycles*, 22(1), 1–10.

Dupin, B., de Rouw, A., Phantahvong, K. B., Valentin, C. (2009). Assessment of tillage erosion rates on steep slopes in northern Laos. *Soil and Tillage Research*, 103(1), 119–126.

Evrard, O., Vandaele, K., van Wesemael, B., Bielders, C.L. (2008). A grassed waterway and earthen dams to control muddy floods from a cultivated catchment of the Belgian loess belt. *Geomorphology,* 100(3-4), 419–428.

Evrard, O., Némery, J., Gratiot, N., Duvert, C., Ayrault, S., Lefèvre, I., Poulenard, J., Prat, C., Bonté, P., Esteves, M. (2010). Sediment dynamics during the rainy season in tropical highland catchments of central Mexico using fallout radionuclides. *Geomorphology*, 124(1-2), 42–54.

Evrard, O., Poulenard, J., Némery, J., Ayrault, S., Gratiot, N., Duvert, C., Prat, C., Lefèvre, I., Bonté, P., Esteves, M. (2013). Tracing sediment sources in a tropical highland catchment of central Mexico by using conventional and alternative fingerprinting methods. *Hydrological Processes*, 27(6), 911–922.

Gateuille, D., Evrard, O., Lefèvre, I., Moreau-Guigon, E., Alliot, F., Chevreuil, M., Mouchel, J.-M. (2014). Mass balance and depollution times of Polycyclic Aromatic Hydrocarbons in rural nested catchments of an early industrialized region (Orgeval River, Seine River basin, France). *Science of the Total Environment*, 470-471, 608-617.

Gourdin, E., Evrard, O., Huon, S., Reyss, J.-L., Ribolzi, O., Bariac, T., Sengtaheuanghoung, O., Ayrault, S. (2014). Spatial and temporal variability of ^{7}Be and ^{210}Pb wet deposition during four successive monsoon storms in a catchment of northern Laos. *Journal of Environmental Radioactivity,* 136, 195–205.

Grangeon, T., Legout, C., Esteves, M., Gratiot, N., Navratil, O. (2012). Variability of the particle size of suspended sediment during highly concentrated flood events in a small mountainous catchment. *Journal of Soils and Sediments*, 12(10), 1549–1558.

Gurnell, A. M. (2007). Analogies between mineral sediment and vegetative particle dynamics in fluvial systems. *Geomorphology*, 89(1-2), 9–22.

Hancock, G. J., Wilkinson, S. N., Hawdon, A. A., Keen, R. J. (2014). Use of fallout tracers ^{7}Be, ^{210}Pb and ^{137}Cs to distinguish the form of sub-surface soil erosion delivering sediment to rivers in large catchments. *Hydrological Processes,* 28, 3855–3874.

He, Q., Walling, D. E. (1996). Interpreting particle size effects in the adsorption of ^{137}Cs and unsupported ^{210}Pb by mineral soils and sediments. *Journal of Environmental Radioactivity,* 30(2), 117–137.

Heidel, S. G. (1956). The progressive lag of sediment concentration with flood waves. *Trans. Am. Geophys. Union*, 37(1), 56–66.

Huisman, N. L. H., Karthikeyan, K. G., Lamba, J., Thompson, A. M., Peaslee, G. (2013). Quantification of seasonal sediment and phosphorus transport dynamics in an agricultural watershed using radiometric fingerprinting techniques. *Journal of Soils and Sediments*, 13(10), 1724-1734.

Huon, S., de Rouw, A., Bonté, P., Robain, H., Valentin, C., Lefèvre, I., Girardin, C., Le Troquer, Y., Podwojewski, P., Sengtaheuanghoung O. (2013). Long-term soil carbon loss and accumulation in a catchment following the conversion of forest to arable land in northern Laos. *Agriculture, Ecosystems and Environment*, 169, 43–57.

Ioannidou, A, Papastefanou, C. (2006). Precipitation scavenging of ^{7}Be and ^{137}Cs radionuclides in air. *Journal of Environmental Radioactivity*, 85(1), 121–36.

Koiter, A. J., Owens, P. N., Petticrew, E. L., Lobb, D. A. (2013). The Behavioural Characteristics of Sediment Properties and their Implications for Sediment Fingerprinting as an Approach for Identifying Sediment Sources in River Basins. *Earth-Science Reviews*, 125, 24–42.

Le Cloarec, M.-F., Bonté, P., Lefèvre, I., Mouchel, J.-M., Colbert, S. (2007). Distribution of ^{7}Be, ^{210}Pb and ^{137}Cs in watersheds of different scales in the Seine River basin: Inventories and residence times. *Science of the Total Environment*, 375(1–3), 125–139.

Manning, R. (1889). On the flow of water in open channels and pipes. *Trans. Inst. Civ. Eng. Ireland*, 20, 161–207.

Mano, V., Nemery, J., Belleudy, P., Poirel, A. (2009). Assessment of suspended sediment transport in four Alpine watersheds (France): influence of the climatic regime. *Hydrological Processes*, (23), 777–792.

Matisoff, G. (2014). ^{210}Pb as a tracer of soil erosion, sediment source area identification and particle transport in the terrestrial environment. *Journal of Environmental Radioactivity, in press.*

Matisoff, G., Wilson, C. G., Whiting, P. J. (2005). The ^{7}Be/^{210}Pb$_{xs}$ ratio as an indicator of suspended sediment age or fraction new sediment in suspension. *Earth Surface Processes and Landforms*, 30(9), 1191–1201.

Meybeck, M., Laroche, L., Dürr, H. H., Syvitski, J. P. M. (2003). Global variability of daily total suspended solids and their fluxes in rivers. *Global and Planetary Change*, 39(1-2), 65–93.

Nagle, G. N., Ritchie, J. C. (2004). Wheat field erosion rates and channel bottom sediment sources in an intensively cropped northeastern Oregon drainage basin. *Land Degradation and Development*, 15(1), 15–26.

Nakamura, R. (1971). Runoff analysis by electrical conductance of water. *Journal of Hydrology,* 14, 197–212.

Olley, J. M., Murray, A. S., Mackenzie, D. H., Edwards, K. (1993). Identifying sediment sources in a gullied catchment using natural and anthropogenic radioactivity. *Water Resources Research*, 29(4), 1037–1043.

Olley, J., Burton, J., Smolders, K., Pantus, F., Pietsch, T. (2012). The application of fallout radionuclides to determine the dominant erosion process in water supply catchments of subtropical South-east Queensland, Australia. *Hydrological Processes*, 27(6), 885–895.

Patin, J., Mouche, E., Ribolzi, O., Chaplot, V., Sengtahevanghoung, O., Latsachak, K. O., Soulileuth, B., Valentin, C. (2012). Analysis of runoff production at the plot scale during a long-term survey of a small agricultural catchment in Lao PDR. *Journal of Hydrology*, 426-427, 79–92.

Pilgrim, D.H., Huff, D.D., Steele, T.D. (1979). Use of specific conductance and contact time relations for separating flow components in storm runoff. *Water Resources Research,* 15, 329–339.

Quinton, J. N., Govers, G., Van Oost, K., Bardgett, R. D. (2010). The impact of agricultural soil erosion on biogeochemical cycling. *Nature Geoscience*, 3(5), 311–314.

Ribolzi, O., Moussa, R., Gaudu, J.-C., Vallès, V., Voltz, M. (1997). Etude des crues de transition entre période sèche et période humide, par traçage naturel sur un bassin versant méditerranéen cultivé. *Comptes Rendus Geosci.* 324, 985–992.

Ribolzi, O., Cuny, J., Sengsoulichanh, P., Pierret, A., Thiébaux, J. P., Huon, S., Bourdon, E., Robain, E., Sengtaheuanghoung O. (2008). Assessment of water quality along a tributary of the Mekong River in a mountainous, mixed land-use environment of the Lao P.D.R. *The Lao Journal of Agriculture and Forestry*, (17), 91–111.

Ribolzi, O., Cuny, J., Sengsoulichanh, P., Mousquès, C., Soulileuth, B., Pierret, A., Huon, S., Sengtaheuanghoung O. (2010). Land use and water quality along a Mekong tributary in northern Lao P.D.R. *Environmental management*, 47(2), 291–302.

Ribolzi, O., Patin, J., Bresson, L. M., Latsachack, K. O., Mouche, E., Sengtaheuanghoung, O., Silvera, N.,Thiébaux, J. P., Valentin, C. (2011). Impact of slope gradient on soil surface features and infiltration on steep slopes in northern Laos. *Geomorphology*, 127, 53–63.

Schuller, P., Iroumé, A., Walling, D. E., Mancilla, H. B., Castillo, A., Trumper, R. E. (2006). Use of Beryllium-7 to Document Soil Redistribution following Forest Harvest Operations. *Journal of Environmental Quality*, 35, 1756–1763.

Sepulveda, A., Schuller, P., Walling, D. E., Castillo, A. (2008). Use of ^{7}Be to document soil erosion associated with a short period of extreme rainfall. *Journal of environmental radioactivity*, 99(1), 35–49.

Sklash, M.G., Farvolden, R.N. (1979). The role of groundwater in storm runoff. *Journal of Hydrology,* 43, 45–65.

Smith, H.G., Dragovich, D. (2009). Interpreting sediment delivery processes using suspended sediment-discharge hysteresis patterns from nested upland catchments, south-eastern Australia. *Hydrological Processes*, 23, 2415–2426.

Syvitski, J. P. M., Vörösmarty, C. J., Kettner, A. J., Green, P. (2005). Impact of humans on the flux of terrestrial sediment to the global coastal ocean. *Science* 308(5720), 376–80.

Tanik, A., Beler Baykal, B., Gonenc, I. E. (1999). The impact of agricultural pollutants in six drinking water reservoirs. *Water Science and Technology*, 40(2), 11–17.

Taylor, A., Blake, W. H., Couldrick, L., Keith-roach, M. J. (2012). Sorption behaviour of beryllium-7 and implications for its use as a sediment tracer. *Geoderma*, 187-188, 16–23.

Taylor, A., Blake, W. H., Smith, H. G., Mabit, L., Keith-Roach, M. J. (2013). Assumptions and challenges in the use of fallout beryllium-7 as a soil and sediment tracer in river basins. *Earth-Science Reviews*, 126, *85-95*.

Thothong, W., Huon, S., Janeau, J.-L., Boonsaner, A., de Rouw, A., Planchon, O., Bardoux, G., Parkpian, P. (2011). Impact of land use change and rainfall on sediment and carbon accumulation in a water reservoir of North Thailand. *Agriculture, Ecosystems and Environment*, 140(3-4), 521–533.

UNESCO (United Nations Educational Scientific and Cultural Organization). (1974). FAO/UNESCO Soil map of the world, 1:5,000,000 Vol.1. Paris: UNESCO.

Valentin, C., Agus, F., Alamban, R., Boosaner, A., Bricquet, J. P., Chaplot, V., de Guzman, T., de Rouw, A., Janeau, J.L., Orange, D., Phachomphonh, K., Podwojewski, P., Ribolzi, O., Silvera, N., Subagyono, K., Thiébaux, J.P., Vadari, T. (2008). Runoff and sediment losses from 27 upland catchments in Southeast Asia: Impact of rapid land use changes and conservation practices. *Agriculture, Ecosystems and Environment*, 128(4), 225–238.

Wallbrink, P. J., Murray, A. S. (1994). Fallout of ^{7}Be in South Eastern Australia. *Journal of Environmental Radioactivity*, 25(3), 213–228.

Walling, D. E. (2012). Beryllium-7: The Cinderella of fallout radionuclide sediment tracers? *Hydrological processes*, 27(6), 830–844.

Walling, D. E., He, Q. (1999). Using fallout lead-210 measurements to estimate soil erosion on cultivated land. *Soil Sci. Soc. Am. J.*, 63, 1404–1412.

Whiting, P. J., Matisoff, G., Fornes, W., Soster, F. M. (2005). Suspended sediment sources and transport distances in the Yellowstone River basin. *Geological Society of America Bulletin*, 117(3), 515–529.

Williams, G. P. (1989). Sediment concentration versus water discharge during single hydrologic events in rivers. *Journal of Hydrology*, 111, 89–106.

Yun-Liang, S., Wu, Y., Mei-E, R. (1985). Hydrological characteristics of the Changjiang and its relation to sediment transport to the sea. *Continental Shelf Research*, 4(1), 5–15.

Figure captions:

Fig. 1: Location of the Houay Xon catchment (top). Houay Xon S10 subcatchment sampling stations and main land uses areas during the study (centre). Location of surface soil, gully and riverbank samples, swamp areas and weather station (bottom).

Fig. 2: ^{7}Be, ^{210}Pb$_{xs}$ and ^{137}Cs stock variations vs. total suspended sediment (TSS) concentration in overland flow exported from the 1-m^2 experimental plot during each of the 45 minutes of the June 1 event. Error bars represent 1σ uncertainty.

Fig. 3: Evolution of rainfall intensity, stream discharge (Q, thicker solid line), total suspended sediment (TSS) concentration, electric conductivity (EC), median particle size (d_{50}), ^{137}Cs, ^{210}Pb$_{xs}$ and ^{7}Be activities and calculated percentage of fresh sediment (F; see text) at upstream station S1 (Houay Pano Stream) during the May 23 flood. River samples: grey circles. Error bars represent 1σ uncertainty.

Fig. 4: Evolution of rainfall intensity, stream discharge (Q, thicker solid line), total suspended sediment (TSS) concentration, electric conductivity (EC), median particle size (d_{50}), ^{137}Cs, ^{210}Pb$_{xs}$ and ^{7}Be activities and calculated percentage of fresh sediment (F; see text) at intermediate station S4 (Houay Pano Stream) during the May 23 flood. River samples: grey circles. Error bars represent 1σ uncertainty.

Fig. 5: Evolution of rainfall intensity, stream discharge (Q, thicker solid line), total suspended sediment (TSS) concentration, electric conductivity (EC), median particle size (d_{50}), ^{137}Cs, ^{210}Pb$_{xs}$ and ^{7}Be activities and calculated percentage of fresh sediment (F; see text) at downstream station S10 (Houay Xon River) during the May 23 flood. River samples: grey circles. Error bars represent 1σ uncertainty.

Fig. 6: Correlations between total suspended sediment (TSS) concentration and ^{7}Be activity at S1 (a) and S4 (b); c: relation between calculated percentage of fresh sediment (F) and calculated percentage of particles derived from surface soil (α) at S10 during the May 23 flood. Regression lines only consider black filled circles (c: peaks samples -white filled circles- are excluded from the regression). Error bars represent 1σ uncertainty.

Fig. 7: Evolution of stream discharge (Q, thicker solid line), total suspended sediment (TSS) concentration (small grey circles), calculated proportions of (1) particles derived from surface/subsurface soil (white/black pie chart) and (2) old/fresh sediment (light-grey/dark-grey pie chart) at S1 (a), S4 (b) and S10 (c) during each stage of the May 23 flood (rise-peak-recession).

Figure1

Click here to download high resolution image

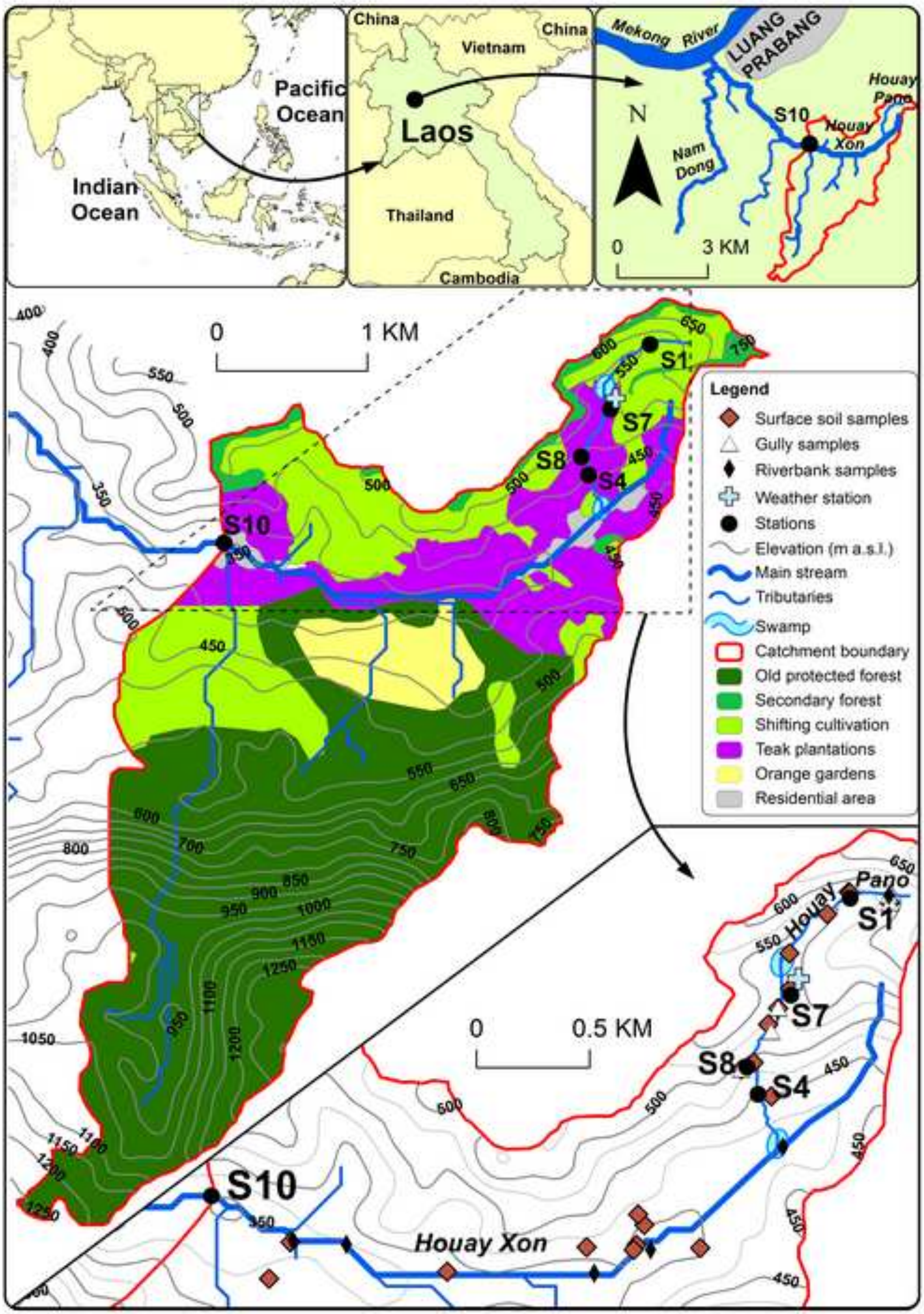

Figure2

Click here to download high resolution image

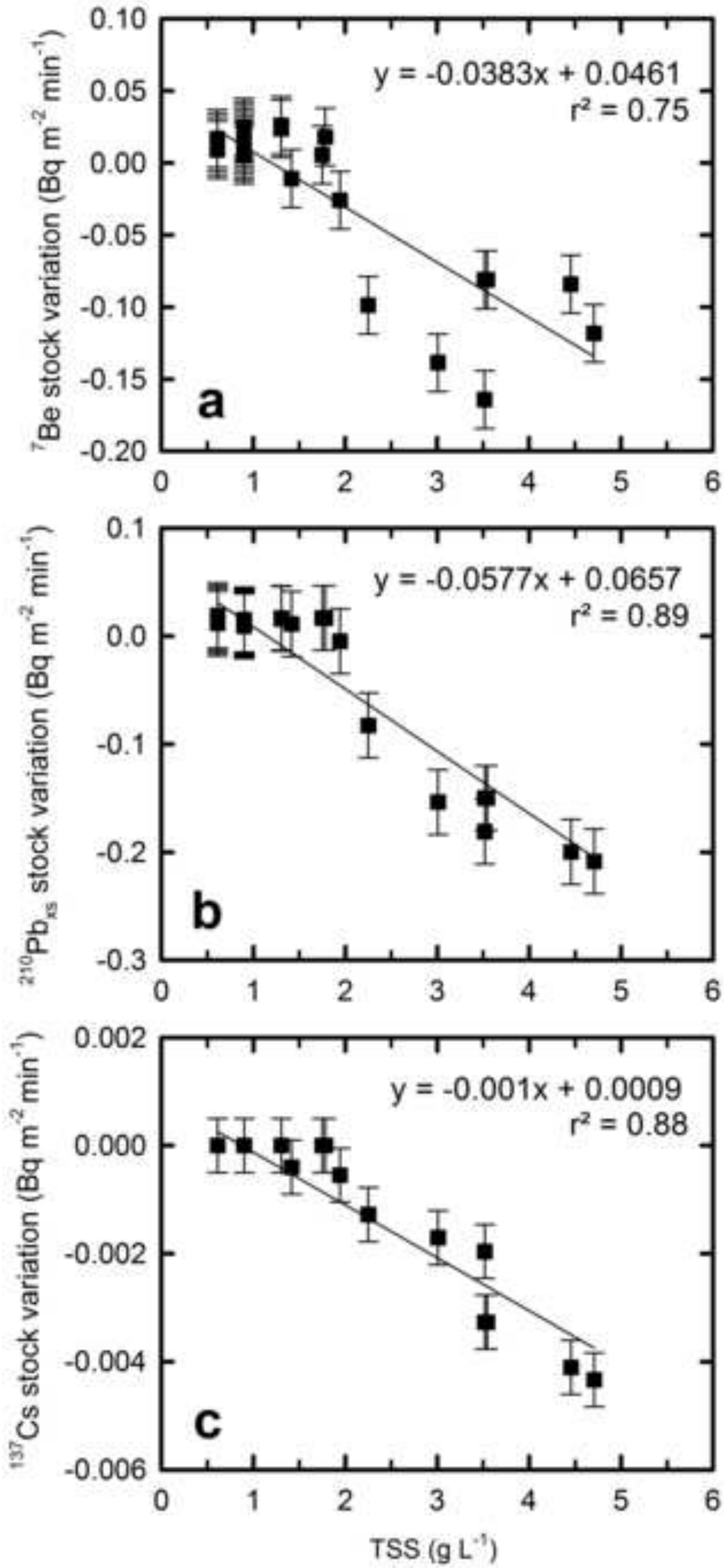

Figure3

Click here to download high resolution image

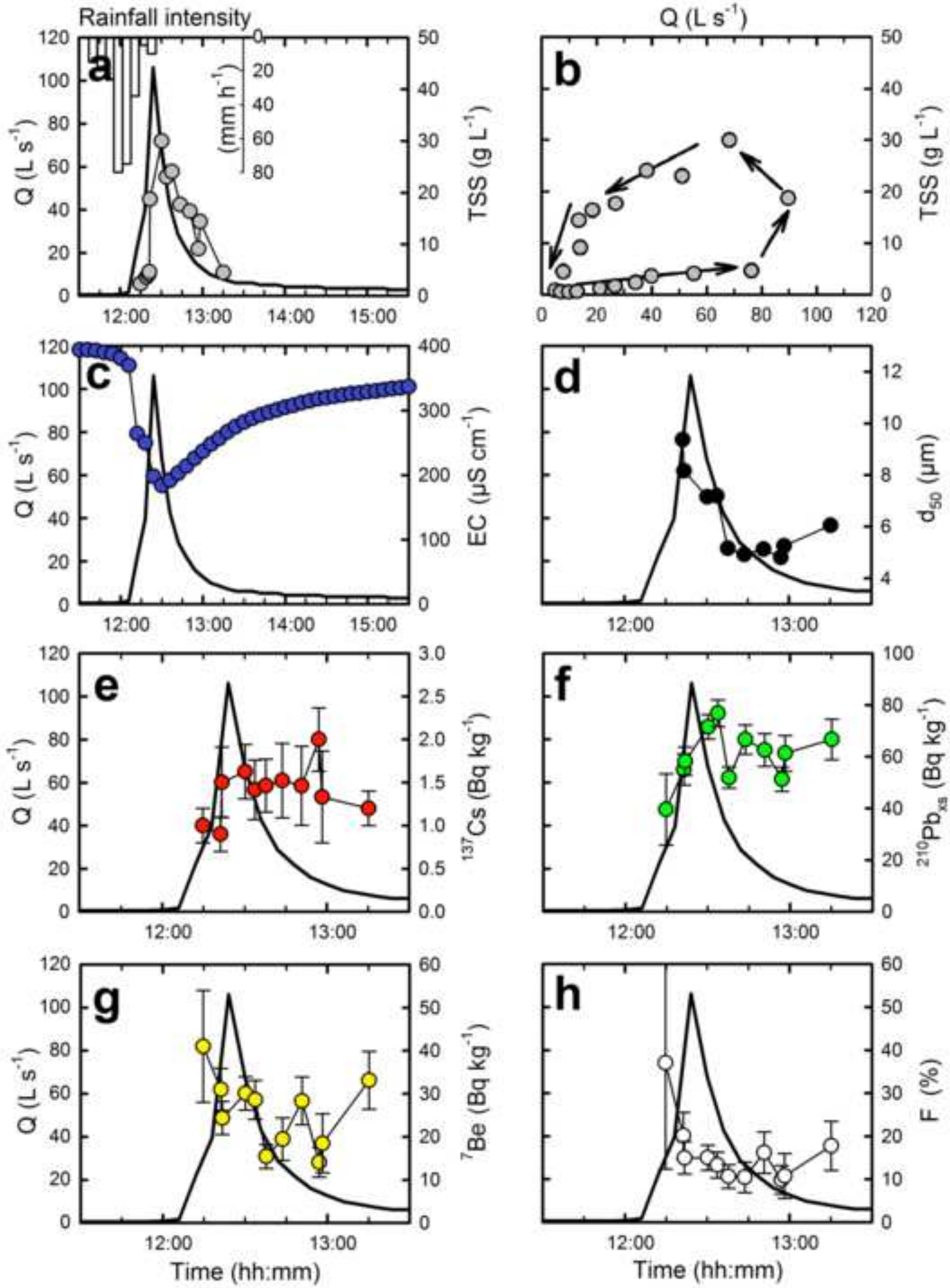

Figure4

Click here to download high resolution image

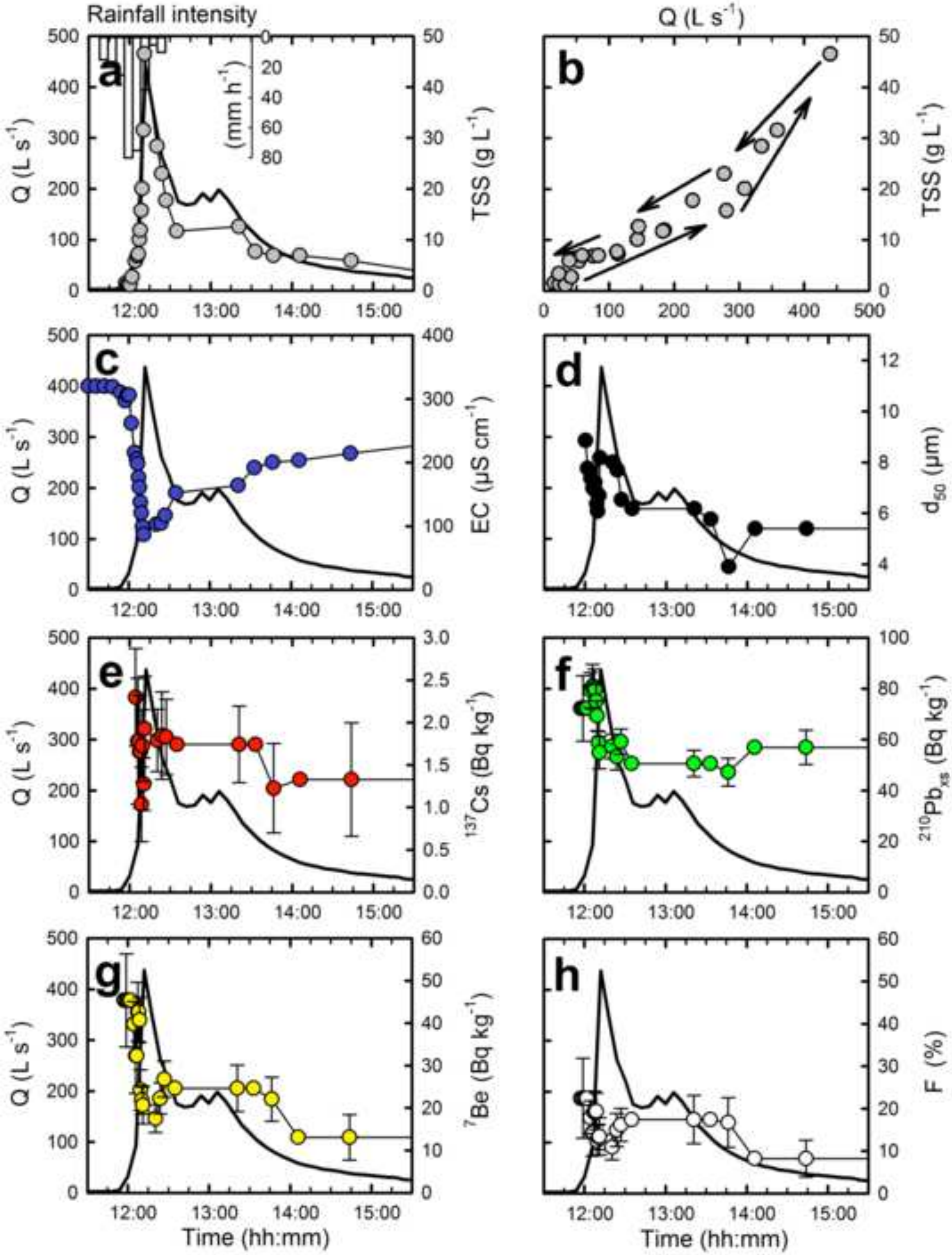

Figure5

Click here to download high resolution image

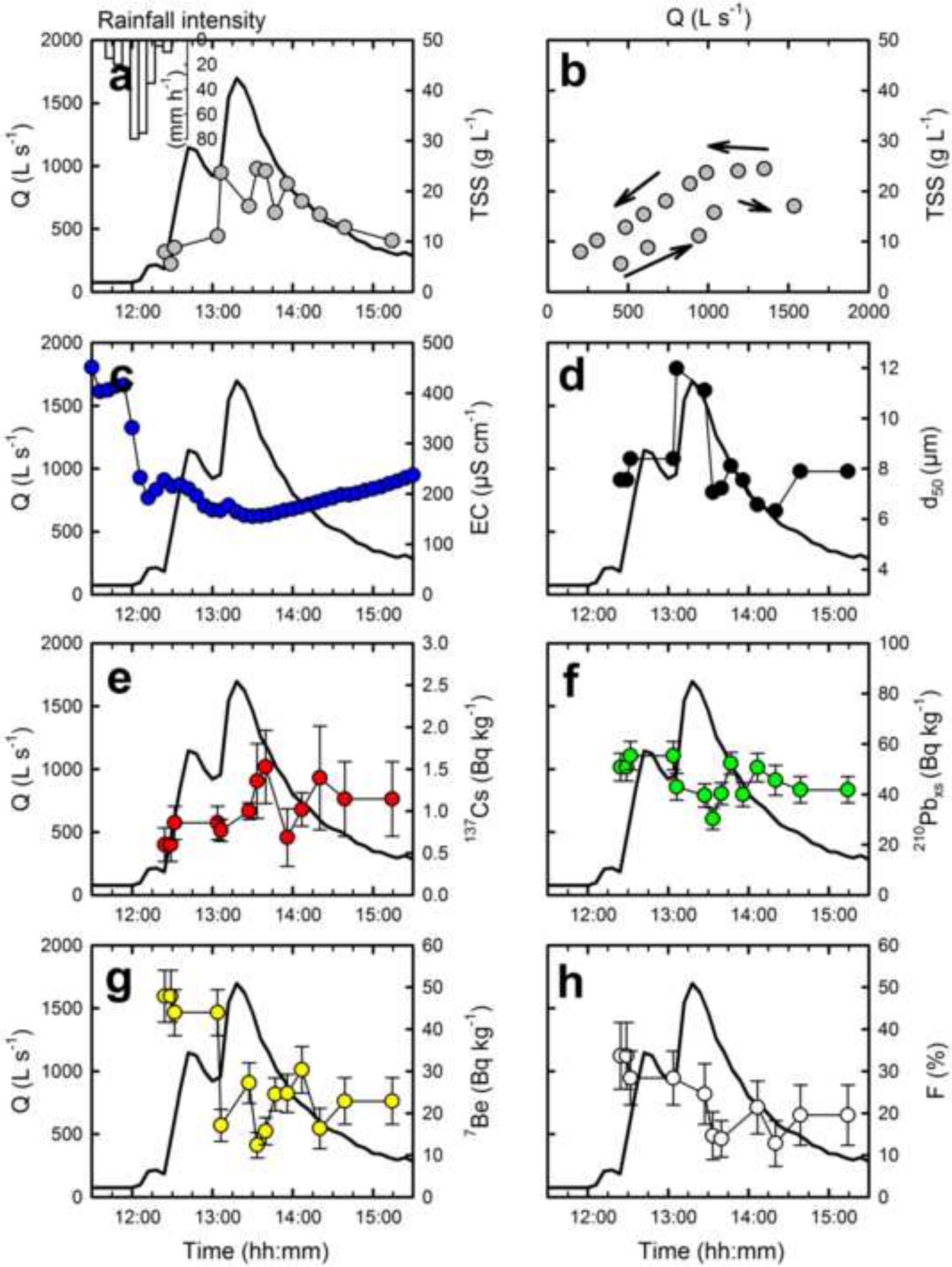

Figure6
Click here to download high resolution image

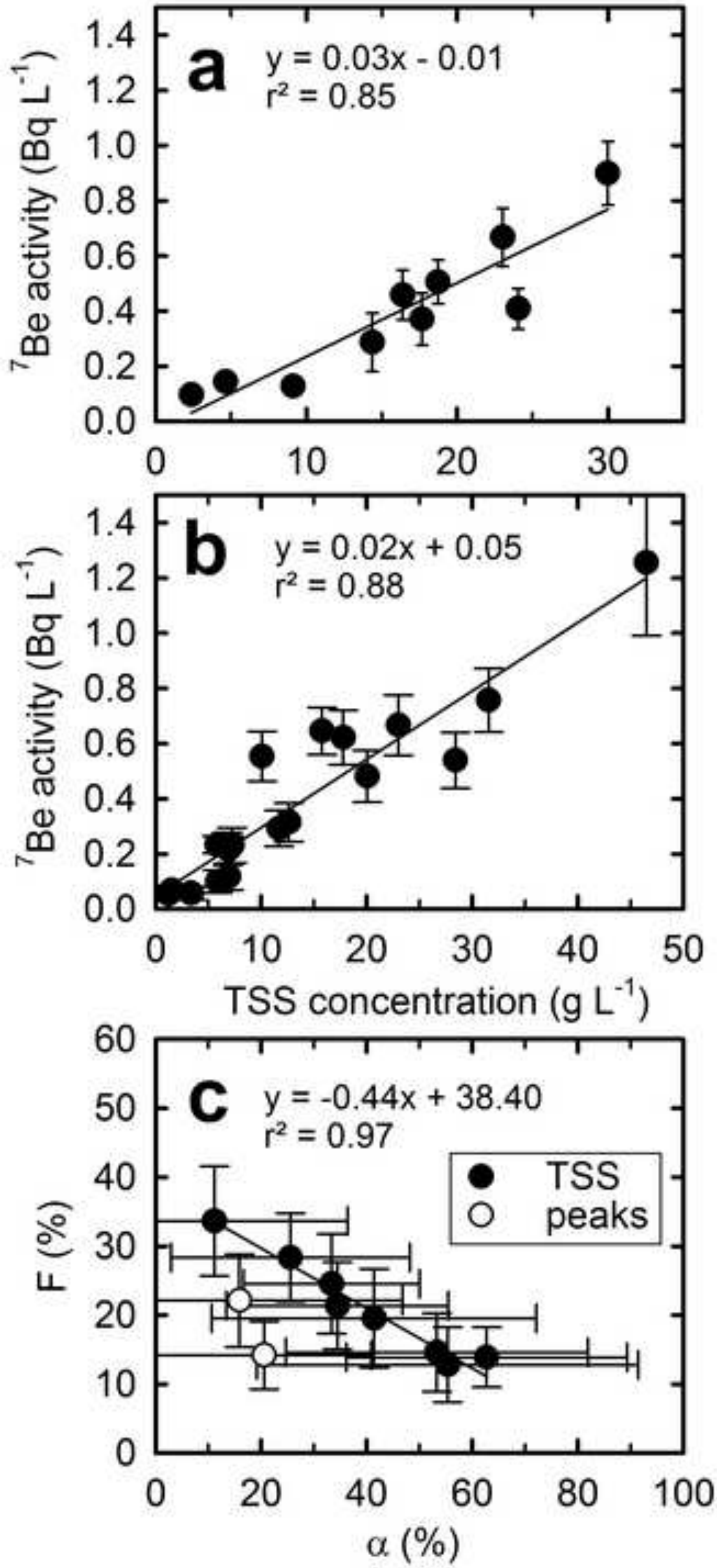

Figure7

Click here to download high resolution image

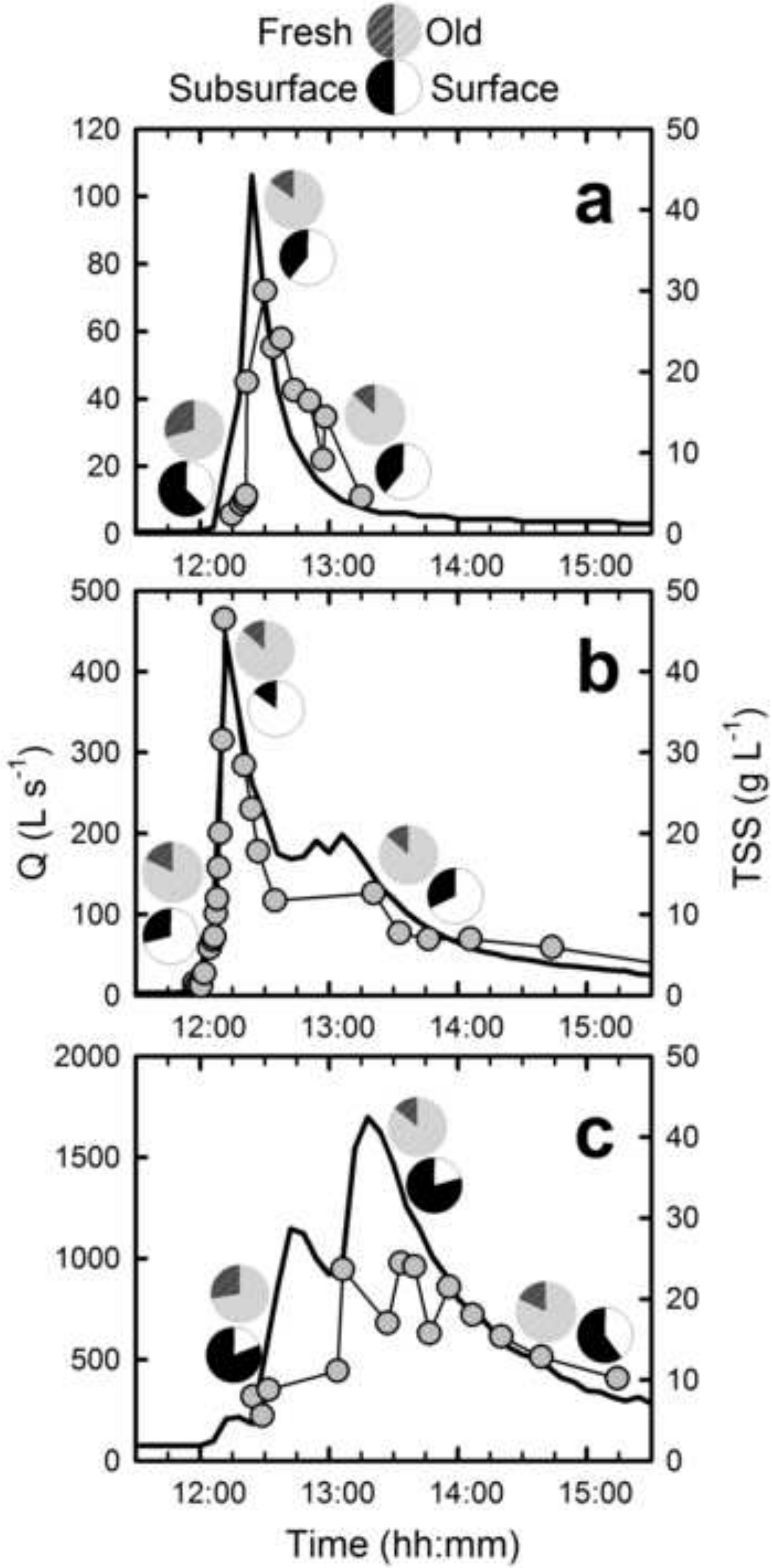

Table 1: Mean radionuclide activity (± 1 standard deviation) for surface soils, gullies and stream bank samples in the Houay Pano and Houay Xon catchments

Location	Number of samples	^{137}Cs (Bq kg^{-1})	$^{210}Pb_{xs}$ (Bq kg^{-1})
Surface soils*	65	2.2 ± 0.9	38 ± 19
Stream banks**	8	0.4 ± 0.3	14 ± 11
Gullies**	6	0.4 ± 0.3	21 ± 27

*Data from Huon et al. (2013) decay-corrected to 2012 and this study (2012), **this study (2012).

Table 2: Sediment budget for the May 23 flood event

Gauging station	S1	S4	S10
Suspended sediment exports (Mg)	2.3	26	130
Catchment surface (km^2)	0.20	0.60	11.6
Sediment yields ($Mg\ km^{-2}$)	11.5	43.3	11.2

Table3

Click here to download Table: Table 3.doc

Table 3: Comparison of $^{7}Be/^{210}Pb_{xs}$ and estimates of fresh sediment proportion (F) compared to literature data

References	**Location**	**Spatial scale**	**Temporal scale**	**$^{7}Be/^{210}Pb_{xs}$**		**F**
				rainfall	sediment	
This study	Northern Laos	3 nested subcatchments (0.2-11.6 km²)	1 storm event	2.8	0.2 – 1.0	8 – 37 %
Evrard et al., 2010	Central Mexico	3 subcatchments (3 – 12 km²)	8 – 18 storms (6 months)	7- 27	2 – 14	10 – 80 %
Bonniwell et al., 1999	ID, USA	Catchment (390 km²) - River (*ca.* 30 km reach)	3 months	*n.a.*	0.3 – 3.8	18 – 96 %
Matisoff et al., 2005	OH; AL; OR, USA	3 catchments (70 km²)	Individual storms (1 year)	13 - 17	1.0 – 1.7	6 – 14 %
Huisman et al., 2013	WI, USA	Catchment (12.4 km²)	7 campaigns (6 months)	3 - 12	0.1 – 5.5	1 – 100 %

n.a. = not available

Graphical Abstract (for review)